Oceanologia (2019) 61, 460—470

Available online at www.sciencedirect.com

ScienceDirect

journal homepage: www.journals.elsevier.com/oceanologia/

ORIGINAL RESEARCH ARTICLE

Gas transfer velocities in Norwegian fjords and the adjacent North Atlantic waters

Hanne M. Banko-Kubis, Oliver Wurl, Nur Ili Hamizah Mustaffa, Mariana Ribas-Ribas *

Center for Marine Sensors, Institute for Chemistry and Biology of the Marine Environment, Carl von Ossietzky University of Oldenburg, Wilhelmshaven, Germany

Received 17 December 2018; accepted 12 April 2019
Available online 1 May 2019

KEYWORDS
Air-sea CO_2 flux;
Gas transfer velocity;
Gas exchange;
Parameterization;
Fjord

Summary We investigated air-sea carbon dioxide (CO_2) transfer in situ to determine the role of wind and turbulence in forcing gas transfer. In situ gas transfer velocities of CO_2 were measured with a floating chamber technique along the Norwegian coast and inside the Sogne- and Trondheimsfjord. Gas transfer velocities were related to wind speed and turbulence, but neither wind speed nor turbulence can satisfactorily predict gas transfer velocity. However, comparison to existing wind-based parameterizations showed that the data from this study have a similar trend. Generally, we measured higher transfer velocities than the parameterizations predict. In the North Atlantic, we measured transfer velocities of up to 54.9 cm h^{-1} versus predicted transfer velocities of 6.3 cm h^{-1} at a wind speed of 3.7 m s^{-1}. In addition, we observed that measurements of transfer velocities at wind speeds below 4 m s^{-1} are higher than predictions. Wind-based parameterizations are lacking data in the low wind regime for validation, and we provide 25 data points for this critical wind speed range. Overall, results indicate that Norwegian fjords and the adjacent North Atlantic are sinks for atmospheric CO_2 during summer, with uptake rates of -9.6 ± 7.6 μmol m^{-2} min^{-1} and -4.1 ± 1.7 μmol m^{-2} min^{-1}, respectively. Due to the low partial pressure of CO_2 in the upper water layer of the stratified fjords (down to 150.7 μatm), the Sogne- and Trondheimsfjord absorb 196 tons of carbon per day during the summer.

* Corresponding author at: Center for Marine Sensors, Institute for Chemistry and Biology of the Marine Environment, Carl von Ossietzky University of Oldenburg, 26382, Wilhelmshaven, Germany. Tel.: +494421944164; fax: +494421944140.
E-mail address: mariana.ribas.ribas@uol.de (M. Ribas-Ribas).
Peer review under the responsibility of Institute of Oceanology of the Polish Academy of Sciences.

ELSEVIER Production and hosting by Elsevier

https://doi.org/10.1016/j.oceano.2019.04.002

1. Introduction

Since the beginning of the Industrial Era, the atmospheric concentration of carbon dioxide (CO_2) has increased by 128 ppm, to approximately 405 ppm in 2017 (Le Quéré et al., 2018). Due to the continuous increase of anthropogenic CO_2 emission and its property as a greenhouse gas, understanding how the ocean absorbs CO_2 is crucial in climate research. For example, about 25% of anthropogenically released CO_2 is taken up by the oceans (Takahashi et al., 2009). It is therefore essential to determine exchange rates of CO_2 between the atmosphere and the ocean for reliable estimation of the global carbon budget.

The CO_2 uptake by the oceans influences water chemistry and leads to ocean acidification because aqueous CO_2 reacts to carbonic acid, bicarbonate, and carbonate ions (Fabry et al., 2008). Ocean acidification, also known as "the other CO_2 problem" (Doney et al., 2009), has become an important field of study to obtain a better understanding of its effect on marine ecosystems (e.g., Hong et al., 2017; Kroeker et al., 2013). With global warming and ocean acidification, two highly debated environmental issues are directly related to the concentration of CO_2 in the atmosphere and the role of the oceans regarding the uptake of CO_2 from the atmosphere.

Whether the ocean acts as a source or a sink for CO_2 depends on the partial pressures of CO_2 in the ocean ($pCO_{2,ocean}$) and the atmosphere ($pCO_{2,atm}$). These partial pressures try to reach an equilibrium; e.g., CO_2 gets dissolved in the ocean if pCO_2 is lower in the water than in the atmosphere, until $pCO_{2,ocean}$ is equal to $pCO_{2,atm}$. The air-sea flux rate of CO_2 depends on the difference of the partial pressures and the gas transfer velocity, also represented by the letter *k*. However, field measurements of gas transfer velocities (k) are challenging (Vachon et al., 2010). For this reason, it is common that k are estimated from parameterizations, solely based on wind speed (Wanninkhof, 2014), to compute fluxes and the global ocean budget (Takahashi et al., 2009). The gas transfer velocity is often parameterized to wind speed because it is well-known that wind-driven near-surface turbulence has a major influence on *k* (Ho et al., 2011; Vachon et al., 2010; Zappa et al., 2003). However, the wide span of wind-based parameterizations indicate that other parameters affect the velocity, such as surfactants, microscale wave breaking, bubbles, rain and biological and chemical enhancement (Garbe et al., 2014). For this reason, field-based measurements of *k* are important to gain a mechanistic understanding of gas exchange processes and to validate parameterizations. Indeed, few studies report the agreement of parameterizations between field studies (Ho et al., 2006; McGillis et al., 2001; Wanninkhof, 1992). While data for moderate wind speeds exist (reviewed by Johnson, 2010), data for low (<4 m s^{-1}) and high (>15 m s^{-1}) wind speeds are lacking (Johnson, 2010; Ribas-Ribas et al., 2018a).

The aim of this study is to contribute to advanced knowledge of air-sea CO_2 exchange velocities under different field conditions. We compared measurements from two Norwegian fjords with transects from the inner parts to the adjacent North Atlantic. A drifting buoy with a floating chamber was deployed to measure in situ *k* and relate them to coherent measurements on turbulence and wind speed. Moreover, we compared the field measurements to existing parameterizations and provide new data to the low wind regime.

2. Material and methods

2.1. Study area

The data were collected during cruise HE491 onboard the r/v *Heincke* from July 8 to 25, 2017. Stations were located in the Sognefjord, the Trondheimsfjord, and along the Norwegian coast, as shown in Fig. 1. The Sognefjord is the world's second-longest (205 km) and deepest (up to 1308 m) fjord (Manzetti and Stenersen, 2010). With a length of 130 km, Trondheimsfjord is the third-largest Norwegian fjord. Fjords are high-latitude estuaries that were formed by glaciers (Syvitski et al., 1987). They typically have deep basins that are separated from the shallower coastal ocean through a sill. The depths of the sill in the Sognefjord and the Trondheimsfjord are 155 m and 195 m, respectively (Mascarenhas et al., 2017). Due to large freshwater inputs, water masses of fjords are commonly stratified (Stigebrandt, 2012). However, only the upper 5 to 15 m of the water column in the Sogne- and Trondheimsfjord show a strong salinity gradient, and the lower water masses are well-mixed. The Sognefjord shows a strong salinity gradient in the surface layers from the inner to the outer fjord due to large freshwater inputs from glacial meltwater (Mascarenhas et al., 2017). Both the Sogne- and Trondheimsfjord are influenced by semi-diurnal tides. The Norwegian coastal current consists of water from the Atlantic Ocean and the North Sea, which mixes with less-saline water masses from the Baltic Sea and the runoff from the Norwegian coast (Sætre et al., 2003). The Norwegian Coastal Current

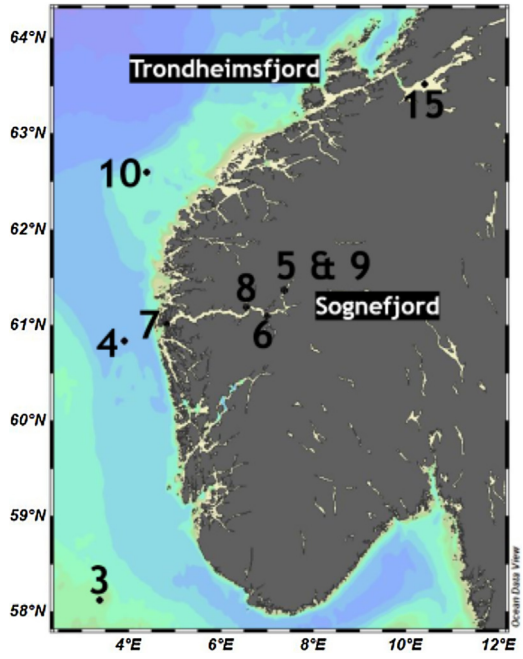

Figure 1 Map of the sampling region during cruise HE491 (southwestern Norway), with all stations that are analyzed in this study. The map was produced using Ocean Data View (Schlitzer, 2017, Ocean Data View, https://odv.awi.de/).

transports heat and less-saline water northwards (Skagseth et al., 2011).

2.2. Field sampling

We deployed an autonomous drifting buoy (*Sniffle*) to measure in situ data on gas transfer velocities (k), which is described in detail by Ribas-Ribas et al. (2018b). To measure the k of CO_2, we used the floating chamber (FC) technique (Kremer et al., 2003) by monitoring pCO_2 over time inside the chamber, floating upside-down within the perimeter of *Sniffle*. *Sniffle* measured pCO_2 in the air ($pCO_{2,atm}$), in the water ($pCO_{2,ocean}$), and in the FC ($pCO_{2,FC}$) with an integrated infrared gas analyzer (IIRGA) (SubCtech OceanPack™, LI-COR LI-840×, range: 0 to 3000 μatm ± 1.5%). $pCO_{2,ocean}$ was measured for 40 min through a 1–2-μm flat-silicone-membrane-equilibrator at a depth of 1.2 m. The upside-down floating chamber had a volume of six liters (diameter: 0.33 m). It was connected to the IIRGA via gas-tight tubing (Swagelok, inner diameter: 6.4 mm). $pCO_{2,FC}$ was measured twice in a sequence, each time over 15 min. From station 5 to station 15, only data from the last 9 min were used due to nonlinearity in the beginning of the cycles. Before recording pCO_2 inside the chamber, air in the floating chamber was exchanged completely by four air pumps (NMP 830 KNDC-B, KNF, flow rate = 2.5 L min^{-1}). $pCO_{2,atm}$ was measured before and after each deployment for one hour on the deck of the r/v *Heincke* while on the station. For later calculations, the mean of all stable $pCO_{2,atm}$ measurements taken on the cruise was used.

Temperature, air pressure, and humidity inside the floating chamber were recorded with a UNI-T UT330C USB data logger at 30-s intervals. The drift of *Sniffle* was monitored by a GPS logger (GT-730FL-S, Canmore, Taiwan) every 10 s. Additionally, *Sniffle* was equipped with two acoustic doppler velocimeters (ADVs) (Nortek) to measure the turbulent kinetic energy (TKE) at approximately 0.1 m depth. The first ADV is located underneath the floating chamber, and the second ADV approximately 0.55 m outside the chamber's perimeter. The inner ADV was equipped with an inertial motion sensor (IMU) (Microstain 3DM-GX3-25-OEM) to correct TKE for the movement of *Sniffle*. A correction was performed according to Kilcher et al. (2016), and data treatment of TKE is described by Ribas-Ribas et al. (2018b).

Conductivity (±0.2%) and temperature (±0.1°C) at 1 m depth were measured from the research catamaran *Sea Surface Scanner* (S^3) (as described in Ribas-Ribas et al. (2017)). Wind speed and air temperature were measured at 3 m height by a weather station mounted on S^3 (Davis Instruments, Vantage Pro2, range wind speed: 0.5 to 89 ± 1 m s^{-1}; range air temperature: −40.0 to 65.0 ± 0.3°C). Wind speed was converted to u_{10} according to Kleemann and Meliß (1993): $u_{10} = (10/H)^{g^*} \times u_H$ (H = 3 m, u_H = wind speed at H, g^* = 0.16 for open water). The wind speed data taken by S^3 were compared to the wind speed measurements on the research vessel (Thies Clima, Windgeber Classic, 0.3 to 50 m s^{-1} ± 2% or 0.3 m s^{-1}) at 23 m height (converted to u_{10} as described above). During deployment, *Sniffle* and S^3 were drifting together with a distance of approximately 20 m to collect data from the same water mass. *Sniffle* and S^3 drifted at a distance of >50 m, but typically >100 m from the research vessel. Air pressure was continuously measured on the research vessel.

2.3. Gas transfer velocities

Gas transfer velocities were calculated according to Ribas-Ribas et al. (2018b). Fluxes in CO_2 (F_{CO_2}) were obtained using the following equation (1):

$$F_{CO_2} = \frac{dp\,CO_2}{dt}\,\frac{V}{S\,T\,R_g}, \tag{1}$$

where $dpCO_2/dt$ is the slope of pCO_2 increase or decrease inside the floating chamber, V is the volume of the floating chamber, S is its surface area, T is the water temperature at 1 m depth, and R_g is the gas constant. Negative fluxes indicate an oceanic uptake of CO_2, while positive fluxes show a release to the atmosphere.

Measurements of $dpCO_2/dt$ were rejected with regression coefficients $R^2 < 0.90$ for the slope. To calculate the gas transfer velocity k_{CO_2}, the following equation (2) was used:

$$k_{CO_2} = \frac{F_{CO_2}}{K(pCO_{2,ocean} - pCO_{2,atm})}. \tag{2}$$

The solubility coefficient K depends on the temperature and salinity (computed from the conductivity) of the seawater and was calculated according to Weiss (1974).

Finally, k_{CO_2} was standardized to k_{660} with the following formula (3):

$$k_{660} = k_{CO_2}\left(\frac{660}{Sc_{CO_2}}\right)^{-n0.5}, \tag{3}$$

Sc_{CO_2} is the temperature-depending Schmidt number (Wanninkhof, 1992) and n the Schmidt number exponent (n = 1/2) (Guérin et al., 2007).

In this study, we obtained 66 accepted k values from 88 measured values in total; i.e., 75% were valid measurements. The error associated with k_{660} and CO_2 fluxes are 13.7% and 10.8%, respectively (Ribas-Ribas et al., 2018b).

2.4. Statistics

Data from the fjords and the North Atlantic were divided into two groups. All stations inside a fjord as well those located at the fjord's mouth were assigned to the group “fjord” due to their direct influence by the characteristics of the fjord system. Stations in the North Atlantic were assigned to the group “oceanic” with a distance of >20 km from the coast (Wurl et al., 2011).

Statistical analysis was performed using R (R Core Team, 2017). Two putative outliers of k_{660} were excluded from further statistical analyses. Correlations between two variables were analyzed using Spearman's correlation analysis. Deming regression was used to find the best fit for two independent variables. Comparison of means was performed using the non-parametric Wilcoxon rank sum test. Analysis of covariance (ANCOVA) was used to compare the means and intercept of the regressions for k with TKE_{ins} and TKE_{out}. A null hypothesis was assumed to be significant when $p < 0.05$.

To parameterize k_{660}'s dependency on u_{10}, quadratic regression analysis was performed. As recommended in

Table 1 Main variables (mean ± standard deviation) measured at each station (abbreviations: station (st.), number (no.), temperature (temp.)).

St.	Day [2017-07-]	Deployment coordinates [start]	Region	Sampling duration [min]	$pCO_{2,ocean}$ [μatm]	No. of k	k_{660} [cm h^{-1}]	Flux [μmol m^{-2} min^{-1}]	u_{10} [m s^{-1}]	TKE_{out} [m^2 s^{-2}]
3	10	58°07′01.286″N 03°22′33.766″E	Oceanic	446	370.9 ± 5.7	11	35.6 ± 9.4	−5.5 ± 0.4	4.7 ± 0.7	0.051 ± 0.010
4	11	60°49′51.938″N 03°55′37.412″E	Oceanic	300	383.7 ± 1.6	7	25.8 ± 3.8	−2.3 ± 0.5	7.0 ± 1.0	0.077 ± 0.013
5	12	61°21′24.455″N 07°22′01.528″E	Inner Sognefjord	397	195.3 ± 15.6	11	10.4 ± 7.5	−11.7 ± 6.3	3.1 ± 1.3	0.017 ± 0.012
6	13	61°05′20.717″N 06°59′56.663″E	Middle-Inner Sognefjord	436	192.0 ± 5.9	11	10.9 ± 3.4	−14.1 ± 4.3	4.9 ± 1.6	0.018 ± 0.011
7	15	61°00′49.630″N 04°49′36.919″E	Outer Sognefjord	144	365.4 ± 3.6	3	24.6 ± 6.0	−4.6 ± 0.7	7.1 ± 0.6	0.050 ± 0.017
8	16	61°11′02.342″N 06°33′36.058″E	Middle-Outer Sognefjord	372	211.1 ± 5.2	2	13.0 ± 1.4	−15.6 ± 1.6	7.8 ± 0.9	0.026 ± 0.004
9	17	61°21′58.579″N 07°22′31.199″E	Inner Sognefjord	376	150.7 ± 21.9	5	10.0 ± 5.6	−16.3 ± 9.9	8.5 ± 1.7	0.031 ± 0.025
10	19	62°35′58.596″N 04°23′27.938″E	Oceanic	388	385.6 ± 3.8	2	45.2 ± 3.2	−2.6 ± 0.5	7.3 ± 0.7	0.066 ± 0.005
15	25	63°31′27.300″N 10°24′39.798″E	Middle Trondheimsfjord	415	336.1 ± 2.7	12	3.2 ± 1.2	−1.1 ± 0.4	1.2 ± 1.0	0.005 ± 0.002

Spiess and Neumeyer (2010), the Bayesian Information Criterion (BIC) was used to compare nonlinear models. Basically, the lower the BIC, the better the fit. The relationship between k_{660}, u_{10}, and TKE was examined with a multiple linear regression (MLR), and the goodness of fit was also evaluated with the BIC (Quinn and Keough, 2009).

3. Results

3.1. Description of general observations

Mean $pCO_{2,atm}$ during the cruise was 398.3 ± 5.3 μatm (N = 1800). Mean $pCO_{2,ocean}$ ranged from 150.7 ± 21.9 μatm (N = 5) in the inner Sognefjord to 385.6 ± 3.8 μatm (N = 2) in the North Atlantic (Table 1). Salinity ranged from 1.32 in the inner Sognefjord (station 5) to 35.14 in the North Atlantic (station 3). $pCO_{2,ocean}$ and salinity show a significant correlation (Spearman correlation, $R \approx 0.83$, $p < 0.0005$). The water temperature in the North Atlantic (14.0 ± 0.3°C) was in general lower than inside fjords (15.5 ± 0.8°C).

Meteorological records are presented in Table S1. The range of u_{10} during the chamber cycles was from 0.43 m s^{-1} (station 15) to 9.65 m s^{-1} (station 9). Wind speed from S^3 and the research vessel are comparable, as shown by correlation analysis (Spearman correlation: $R \approx 0.93$, $p < 0.0001$). For further data analysis, we used wind speeds from the catamaran S^3 due to close proximity to *Sniffle*—i.e., < 20 m.

3.2. *k* parameterizations

Fig. 2 shows k_{660} without error bars for better clarity. The same data with error bars are shown in Figure S1. Mean k_{660} values from all oceanic North Atlantic measurements are, at 33.1 ± 9.5 cm h^{-1}, significantly higher than those from fjords at 9.6 ± 7.0 cm h^{-1} (Wilcoxon rank sum test, $p < 0.005$). The highest mean k_{660} value was measured at station 10 in the North Atlantic (45.2 ± 3.2 cm h^{-1}, N = 2), while lowest mean k_{660} was found at station 15 in the Trondheimsfjord (3.2 ± 1.2 cm h^{-1}, N = 12), associated with the lowest mean wind speed of 1.2 ± 1.0 m s^{-1}.

Fig. 2 shows that k_{660} values from this study generally fit to existing parameterizations, but values measured in the fjords show a better fit than the values from the North Atlantic. However, scattering of the values does not allow choosing a single parameterization for the best fit. Therefore, we performed quadratic regression for our data (Fig. 2), as recommended in Wanninkhof (2014). Regression of all our data ($k_{660} \approx 0.176 \times u_{10}^2 + 12.21$, N = 64, BIC ≈ 532.3), and the data from fjords ($k_{660} \approx 0.138 \times u_{10}^2 + 3.60$, N = 44, BIC ≈ 293.9) lie in the range of the existing parameterizations (McGillis et al., 2001; Raymond and Cole, 2001; Wanninkhof, 2014), although they predict higher k_{660} values at low wind speeds but a smaller slope. Regression for oceanic data ($k_{660} \approx -0.240 \times u_{10}^2 + 41.09$, N = 20, BIC ≈ 151.8) has a negative slope which does not accord to what is known from the literature. Therefore, we assume that the regression shows a wrong trend due to the limited amount of data in a small range of wind speed and other factors than wind affecting k_{660} in the North Atlantic. It is noticeable that nearly all North Atlantic measurements revealed higher k_{660} values than predicted from the wind-based parameterizations. Donelan and Drennan (1995) measured k_{660} in a similar high range in Lake Ontario (see Fig. 3 in Donelan and Drennan, 1995). Though several k_{660} values fit best to the curve of Raymond and Cole (2001), probably because data used in Raymond and Cole (2001) were taken in rivers and estuaries and about 33% of their data were measured with the floating chamber technique similar to this study. However, our study provides

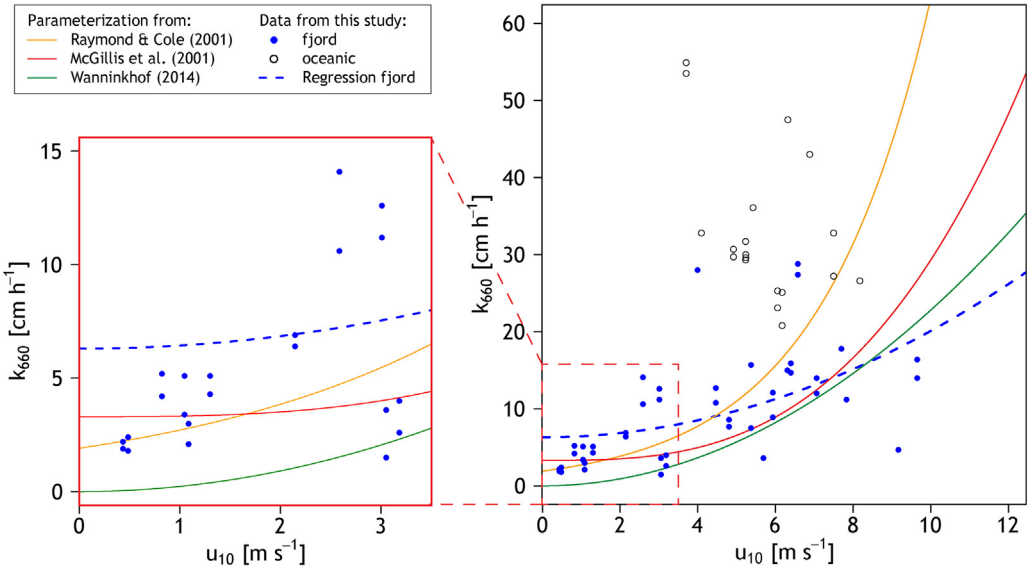

Figure 2 Gas transfer velocities scaled to a Schmidt number of 660 (k_{660}) and a Schmidt number exponent of −0.5 for the fjord (solid blue circles) and the oceanic stations (open data points) vs. a wind speed (u_{10}) scatterplot in comparison to other parameterizations (McGillis et al., 2001; Raymond and Cole, 2001; Wanninkhof, 2014). The data in the red box are the empirical data added in the lower wind speeds, where known parameterizations fall short. (For interpretation of the references to color in this figure legend, the reader is referred to the web version of this article.)

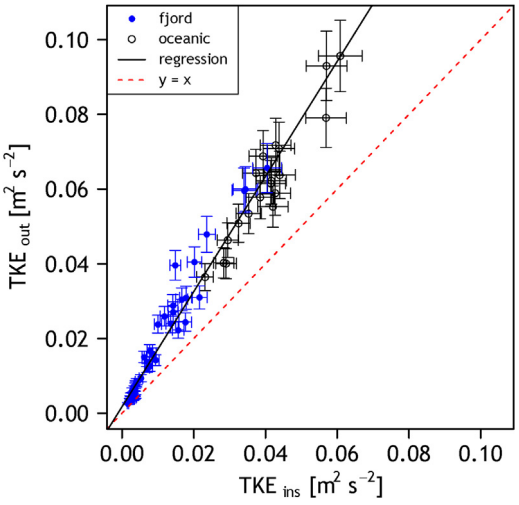

Figure 3 Relationship between Turbulent Kinetic Energy (TKE) inside (TKE_{ins}) and outside (TKE_{out}) the floating chamber for the fjord stations (solid blue circles) and oceanic stations (open data points). The black line represents the Deming regression ($TKE_{out} \approx 1.54 \times TKE_{ins} + 0.0018$). The line of perfect agreement (1:1 line) is shown in red. (For interpretation of the references to color in this figure legend, the reader is referred to the web version of this article.)

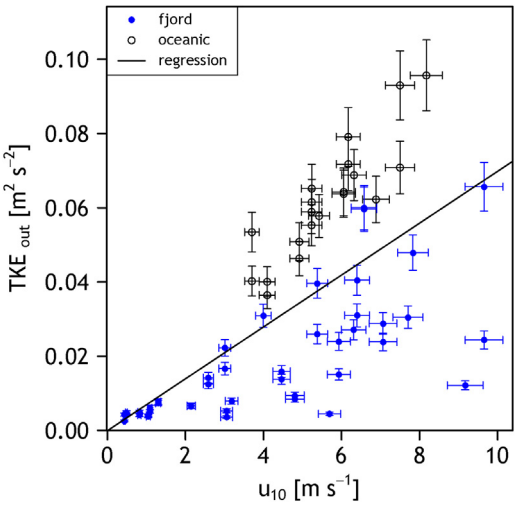

Figure 4 Relationship between wind speed at 10 m (u_{10}) and TKE_{out} for the fjord stations (solid blue circles) and oceanic stations (open data points). The black line represents the Deming regression ($TKE_{out} \approx 0.007 \times u_{10}$). (For interpretation of the references to color in this figure legend, the reader is referred to the web version of this article.)

k_{660} values ($N = 25$) for the low wind regime (0 to 4 m s^{-1}), while wind-based parameterizations typically lack empirical data for low wind speeds. Our data show that the gas transfer velocity is not as close to zero as predicted by parameterizations for the low wind regimes (<4 m s^{-1}), as shown in Fig. 2.

3.3. TKE measurements

Fig. 3 shows that TKE outside *Sniffle's* structure (TKE_{out}) was higher for nearly all measurements. On average, TKE_{out} was approximately 1.5 times higher than TKE below the floating chamber (TKE_{ins}) (Deming regression: $TKE_{out} \approx 1.54 \times TKE_{ins} + 0.0018$, $N = 64$). TKE measurements from the two different measuring points (TKE_{ins} and TKE_{out}) have a significant dissimilarity (Wilcoxon rank sum test; $p < 0.005$). Additionally, TKE measured in the fjords was significantly lower compared to the TKE measured in the North Atlantic (Wilcoxon rank sum test; $p < 0.005$).

ANCOVA showed that the slopes between k_{660} and both TKE measurements were similar (F-test of slopes, $p \approx 0.59$, $F \approx 0.29$), and thus any interference of the chamber on near-surface turbulence was minimal and did not interfere with the CO_2 flux. Because TKE_{ins} and TKE_{out} have a similar slope, only TKE_{out} will be shown in the further analysis for simplicity.

Although there is a significant correlation between wind speed and turbulence (Spearman correlation, TKE_{ins}: $r \approx 0.72$, TKE_{out}: $r \approx 0.74$, $p < 0.001$), higher turbulence did not always result in higher wind speeds (Fig. 4). For example, in the fjords, TKE does not reach high values at higher wind speeds (e.g., >8 m s^{-1} at station 9), probably due to the lower fetch. On the other hand, at low wind speeds, TKE tended to be in its lowest range. The relationship between k_{660} and TKE_{out} is shown in Fig. 5. We observe two clear data groups, one for measurements in the fjords with

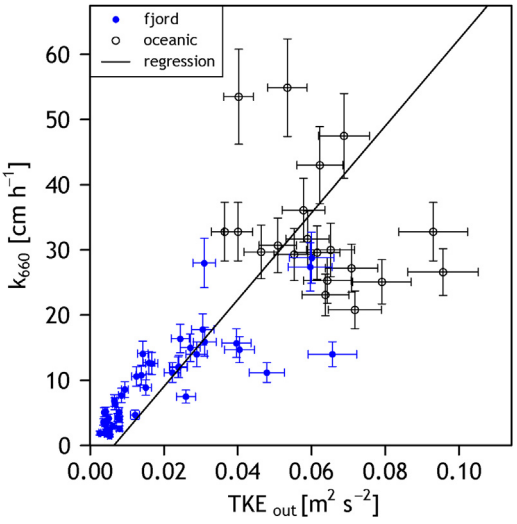

Figure 5 Relationship between TKE_{out} and k_{660} for the fjord stations (solid blue circles) and oceanic stations (open data points). The black line represents the Deming regression ($k_{660} \approx 665.95 \times TKE_{out} - 4.26$). (For interpretation of the references to color in this figure legend, the reader is referred to the web version of this article.)

TKE lower than 0.04 m^2 s^{-2} and another with higher TKE and k_{660} observed in the North Atlantic.

3.4. Combined impact of wind speed and turbulence

To investigate the combined effect of u_{10} and TKE on k_{660}, MLR was performed with u_{10} and TKE_{out}: $\log(k_{660}) \approx 1.35$ (± 0.13)

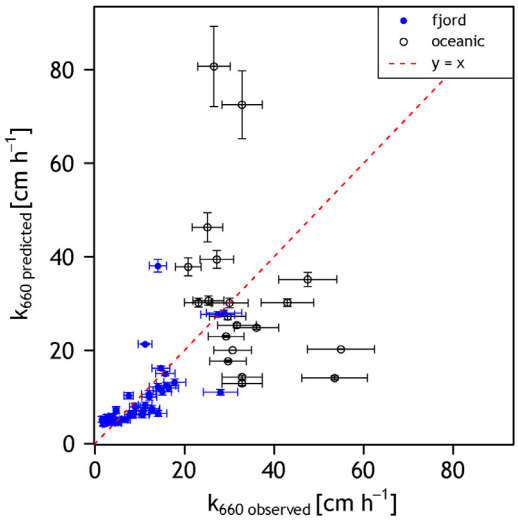

Figure 6 Relationship between observed k_{660} and predicted k_{660} from the multiple linear regression for the fjord stations (solid blue circles) and oceanic stations (open data points). The line of perfect agreement (1:1 line) is shown in red. (For interpretation of the references to color in this figure legend, the reader is referred to the web version of this article.)

+ 0.05 (±0) × u_{10} + 27.51(±2.53) × TKE_{out}; BIC ≈ 121.45. Due to the lower BIC values, MLR explains the relationships between k, u_{10}, and TKE better than the quadratic regression between k_{660} and u_{10} (see Section 3.2). Fig. 6 shows the relationship between observed and predicted k_{660} values from multiple linear regression with TKE_{out} and TKE_{ins}. It is clear that there is a bilateral trend and that there is less scattering in the area of low k_{660} values.

3.5. Revisiting a single station

We deployed *Sniffle* twice in the inner part of the Sognefjord; i.e., on the 12th and 17th of July 2017 (stations 5 and 9) (Table 1). The k were insignificantly different (*t* test, *p* value ≈ 0.91) at station 5 (10.4 ± 7.5 cm h^{-1}) and station 9 (10.0 ± 5.6 cm h^{-1}), although the wind speed was significantly higher (Wilcoxon rank sum test, p value < 0.005) at station 9 (8.5 ± 1.7 m s^{-1}) compared to station 5 (3.1 ± 1.3 m s^{-1}). The dominating wind direction on both days was west-northwest. Mean TKE under the chamber was 0.06 m^2 s^{-2} (station 5) and 0.11 m^2 s^{-2} (station 9). Salinity was low on both days and ranged from 1.7 to 4.0 (station 5: 5.88 ± 4.75; station 9: 3.37 ± 0.29) (Table S1). $pCO_{2,ocean}$ was *significantly higher (test,p* at station 5 (195.3 ± 15.6) compared to station 9 (150.7 ± 21.9). Ancillary data, like surfactants reported in Mustaffa et al. (submitted) and chlorophyll-*a* (data not shown), were similar at both stations, not explaining similar k_{660} values of the two wind regimes.

4. Discussion

4.1. Aqueous pCO_2

This study shows that the Norwegian fjords might play an important role as sinks for atmospheric CO_2. Due to the high inflow of cold, fresh glacial meltwater, they have low pCO_2 values. Even though estuaries are known to be a source of CO_2 (Cai, 2011), other studies concluded that fjords may play an important role in global carbon cycling (Meire et al., 2015; Smith et al., 2015). For example, Meire et al. (2015), who investigated an Arctic fjord, calculated CO_2 fluxes and reported that the fjord act as sink for CO_2 throughout the year. Our correlation of aqueous pCO_2 with salinity agrees with Torres et al. (2011), who found a correlation between aqueous pCO_2 and salinity, as well as aqueous pCO_2 and water temperature. In addition, surface CO_2 saturation changes with the season due to differences in biological activity or the frequency of storm events. For example, Torres et al. (2011) observed a maximum saturation of CO_2 in winter, while aqueous pCO_2 was lower in spring and summer. In our study, photosynthetic efficiency was low (data not presented), suggesting that we conducted our measurements after summer bloom.

4.2. Modification of k parameterization

In this study, it was inappropriate to parameterize k solely by wind speed. Existing wind-based parameterizations do not fully explain k in the fjords or in the North Atlantic. The fact that we measured similar k values at the same location under different wind and turbulence regimes (Section 3.5) clearly indicates that the wind speed or turbulence alone could not explain the variability in k. Interestingly, k values for stations 5 and 9 were close to 10 cm h^{-1} and consistent with a reported non-zero intercept (Ribas-Ribas et al., 2018a; Zhang and Cai, 2007) suggesting a background k in certain conditions.

For example, multiple linear regression of our data with wind and turbulence explained the variations better but with some remaining discrepancies. As Jeffery et al. (2010) already suggested, other influencing parameters, such as surfactants and rising bubbles, should be taken into account to develop a complete model for k. For example, the effect of surfactants was recently investigated in a wind-wave tunnel with a reduction of k by up to 60% with increasing surfactant concentrations (Ribas-Ribas et al., 2018b). However, this has not been achieved yet due to challenges in field measurements and the high complexity of air-sea gas transfer and its description in models. Hence, parameterizations with one variable, for example, wind or turbulence, have been used as an approximation. Nevertheless, it should be considered if parameterizations are valid in general terms and how good such approximations are. For example, the data from our study show that there are differences between estuaries and oceanic CO_2 transfer velocities. Therefore, we agree with Raymond and Cole (2001) that parameterizations of k should be distinguished for estuaries and open ocean environments.

Although there are still some discrepancies, our data show that a parameterization with TKE explains more variance of k compared to parameterizations with wind speed alone. That is illustrated in Fig. 5, showing that higher turbulence is not always related to higher wind speeds. This is in agreement with Zappa et al. (2007) and Esters et al. (2017), suggesting that near-surface turbulence is the primary driving mechanism for k at low to moderate wind speeds ($u_{10} < 10$ m s^{-1}). Therefore, we propose to use TKE instead of the dissipation rate (ε) because the calculation of ε is a parameter in a

spectral fit and not straightforward to determine. A good fit is critical for ε to be a good proxy for k. TKEs are easier to calculate for scientists from a wider range of research backgrounds, as determination of TKE does not require the computation of the fit and can be directly calculated from the dolfyn routine (https://lkilcher.github.io/dolfyn/). Moreover, TKE and ε show a similar trend (e.g., Figures 14B and D in Kilcher et al. (2017)).

Regarding parameterizations with wind speed, Wanninkhof (2014) highlighted the strong agreement between existing quadratic parameterizations. In terms of the data collected in this study, we suggest adding an intercept to the parameterization because we observed higher k at low wind speeds than the quadratic parameterizations predict (see Fig. 3). Our statement agrees with other studies (McGillis et al., 2001; Raymond and Cole, 2001; Ribas-Ribas et al., 2018a) who also detected higher k in the range of 0 to 4 m s^{-1}, based on direct covariance, gas tracer measurements and the floating chamber.

4.3. Other factors and processes potentially affecting gas transfer velocities

There are several other factors apart from wind speed or turbulence, that have an impact on the CO_2 transfer velocity as described by Wanninkhof et al. (2009). These additional factors might explain the high values for k we detected in the North Atlantic: values which are higher than other in situ data from the literature (Ho et al., 2006; McGillis et al., 2001). Such a discrepancy can have various reasons:

(a) *Fetch*: In the fjord systems, correlations between turbulence and wind speed are less significant (Fig. 4) than the open ocean, which could be due to the different wind fetch in the narrow fjords. On the open surface at the oceanic stations, high wind speeds have a more pronounced effect on near-surface turbulence as well as the formation of waves and therefore the presence of bubbles and sea spray.
(b) *Surfactants*: The occurrence of surface slicks, a sea surface phenomenon of wave-damping areas visible as lighter patches (Romano, 1996) can reduce near-surface turbulence and thus have a profound effect on the reduction of k (Frew et al., 2002). In different experiments, the suppression of k due to surfactants was investigated. In in situ measurements, k was found to decrease by 62% in the presence of surface films (Mustaffa et al., in preparation), which is in agreement with Pereira et al. (2016), who found 14–51% k suppression (ex-situ) and Bock et al. (1999), who performed lab experiments (k reduction up to 60%).
(c) *Water-side convection*: Water-side convection can greatly increase gas transfer velocity (Rutgersson and Smedman, 2010), such as surface cooling and resulting convective mixing enhancing the oceanic uptake of CO_2. Andersson et al. (2017) found strong enhancement of CO_2 exchange in Arctic fjords and highlight the importance of this observation for Arctic fjords and coastal waters. In the case of this study, high k values were found at the oceanic stations but not inside the fjords. That can have several reasons. In contrast to Andersson et al. (2017) who conducted their measurements in the high Arctic in March, we sampled in temperate fjords in summer. Furthermore, a deep mixed layer depth is important for high water-side convection. The observed fjords have a highly stratified water column during summer, while high turbulence might have caused a deep mixed layer depth in the North Atlantic.
(d) *Temporal and spatial variability*: Sampling for this study took place in summer, while other parameterizations include measurements at other seasons or over a complete seasonal cycle. Biogeochemistry of the sampled water can largely differ depending on the sampling time and region. For example, McGillis et al. (2001) reported gas fluxes for the open North Atlantic during June, with the potential presence of a phytoplankton bloom.
(e) *Technology*: The use of different techniques to measure k may further explain discrepancies between different data sets as we further explain in Section 4.5.

Clearly, the bilateral trend of our data indicates that more research is needed in the future to identify the impact of factors that might affect k.

4.4. CO_2 air-sea fluxes in fjords and adjacent oceans

As mentioned above, the results show that fjords have a large CO_2 absorption capacity: Mean flux for fjords was -9.6 ± 7.6 μmol m^{-2} min^{-1} ($N = 44$) and -4.1 ± 1.7 μmol m^{-2} min^{-1} ($N = 20$) for the North Atlantic. Overall, our study reveals that the Sogne- and Trondheimsfjord absorb 196 tons of carbon per day (C d^{-1}) during summer, based on the fjords' area and assuming that our measured fluxes are representative across the whole area. Chilean fjords also act as a CO_2 sink during warm weather in a similar range (-9.5 μmol m^{-2} min^{-1}) (Torres et al., 2011). The sampling locations in the North Atlantic are located north of 54°N, which Bozec et al. (2005) defined as the northern North Atlantic. Bozec et al. (2005) reported that the northern North Atlantic acts as a sink for atmospheric CO_2 within a similar range to our observation — i.e., -1.7 to -2.6 μmol m^{-2} d^{-1} — during late summer.

Turbulence inside the two fjords was lower than in the North Atlantic, with averaged TKE inside the fjords of 0.010 ± 0.009 ($n = 44$) and 0.040 ± 0.009 ($n = 20$) in the North Atlantic, consequently causing lower k in the fjords. Large absorption with low k could only happen with very large ΔpCO_2, which drives the large uptake of CO_2 inside the fjords (Table 1).

Regarding the difference in k between estuarine and open-ocean measurements, we observed the reverse trend of Raymond and Cole (2001). They detected higher k values in estuaries than in the open ocean at the same wind speed. A possible reason could be that they investigated estuaries from North American rivers that already run great distances, whereas the glacial meltwater in the fjords has not been exposed to the atmosphere for long and was less influenced by humans.

4.5. Possible limitations of the floating chamber technique

Measuring k remains a challenging task of today's ocean scientists. Three techniques are widely used: the floating

chamber technique (as in this paper), eddy covariance, and the dual tracer technique (Wanninkhof et al., 2009). The floating chamber technique is a direct measurement and offers a high spatial and temporal resolution, which is needed to understand high ocean variability. Eddy covariance and dual-tracer gases have a much larger spatial footprint (>1 km^2) and temporal scales (>12 h). Furthermore, their data analysis requires more expertise, and they are challenging to apply from research vessels due to the ship's movement (eddy covariance) and need to track the plumes of injected tracer gases (dual tracer gases). The floating chamber technique has been criticized because it covers the water surface and thus has a direct impact on the flux measurement (Borges et al., 2004). The wind is eliminated from the chamber's interior, and the chamber can cause mass boundary perturbations (Vachon et al., 2010). Our data showed that the chamber did not create artificial turbulence as is assumed in Tokoro et al. (2007), as the measurements inside the floating chamber (TKE_{ins}) were not higher than outside (see Fig. 4). To the contrary, turbulence outside the chamber was 1.5 times higher than inside. It could be that the chamber was dampening the movement of the inner ADV or that the outer ADV moved more due to leverage and we only corrected for *Sniffle*'s movement with the inner ADV, where the IMU is located. In our case, we did not correct for different turbulence because the two regressions did not intersect; i.e., they had similar slopes (Ribas-Ribas et al., 2018b). Additionally, no light penetrates the chamber's walls. This might shift the dominant metabolism under the chamber from photo- to heterotrophy and thereby change the gas transfer. However, the switch from photo- to heterotrophy requires more time on a scale of hours (Pringault et al., 2007) than the measuring cycle from *Sniffle* (15 min). Another critique is that the temperature and pressure inside the chamber might also change during one measuring cycle. In our case, both factors slightly changed by a maximum of 31 and 0.6%, respectively (Table S1), but not always in the same direction, making it challenging to determine their influence on k measurements. Moreover, the partial pressure inside the chamber is measured over a period of time (in our case 15 min), so the value for pCO_2 in the air inside the chamber changes over that time. We achieved good slopes to calculate k with a strict quality control scheme, but changing partial pressure may also shift the slopes during deployment. Another source of error, shared with the eddy covariance and dual-tracer techniques is, that *Sniffle* measures $pCO_{2,ocean}$ at 1.2 m depth (due to the size of the pCO_2 sensor) and not close to the sea surface, where the exchange occurs. This could be a possible explanation of why we observed occasionally negative k with higher $pCO_{2,ocean}$ than $pCO_{2,atm}$. Due to the stratification of the water, the gradient from 1.2 m water depth to the surface could have been significant with much lower $pCO_{2,ocean}$ at the sea surface, and therefore the surface layer may act as a source of CO_2 with negative k values. For future measurements, we recommend measuring aqueous pCO_2 closer to the water surface and comparing the floating chamber measurements in situ to another method (e.g., the eddy covariance and dual gas tracer techniques).

5. Conclusion

Overall, our study provides a better understanding of k, especially at low wind speeds. The data from this study show that there are differences between estuaries and oceanic CO_2 transfer velocities. Therefore, we agree with Raymond and Cole (2001) that parameterizations should be distinguished for estuaries, coastal areas, and open ocean. Our data from two marine environments show that wind-based parameterizations of k cannot fully explain both regimes. Our data suggest that a parameterization with TKE would explain more variance of k than parameterizations with wind speed. Additionally, we conclude that fjords might play an important role as a sink for CO_2 due to low aqueous pCO_2 values driving flux. Measurements in the North Atlantic revealed lower uptake rates of CO_2 but higher transfer velocities due to closer conditions to equilibrium. Therefore, new in situ approaches to parameterize k with multiple parameters (e.g., turbulence) should be developed to verify or modify existing parameterizations.

Acknowledgements

This work was funded by the European Research Council's (ERC) PASSME project (grant no. GA336408). The authors would like to thank the captain and crew of the r/v *Heincke* for their supportive work on board. We also thank the scientific crew onboard r/v *Heincke* for their help in the deployments. We thank Marcus Plath and Tiera-Brandy Robinson for editorial assistance.

Appendix A. Supplementary data

Supplementary data associated with this article can be found, in the online version, at doi:10.1016/j.oceano.2019.04.002.

References

Andersson, A., Falck, E., Sjöblom, A., Kljun, N., Sahlée, E., Omar, A. M., Rutgersson, A., 2017. Air-sea gas transfer in high Arctic fjords. Geophys. Res. Lett. 44 (5), 2519–2526, http://dx.doi.org/10.1002/2016GL072373.

Bock, E.J., Hara, T., Frew, N.M., McGillis, W.R., 1999. Relationship between air-sea gas transfer and short wind waves. J. Geophys. Res.-Oceans 104 (C11), 25821–25831, http://dx.doi.org/10.1029/1999jc900200.

Borges, A.V., Delille, B., Schiettecatte, L.S., Gazeau, F., Abril, G., Frankignoulle, M., 2004. Gas transfer velocities of CO_2 in three European estuaries (Randers Fjord, Scheldt, and Thames). Limnol. Oceanogr. 49 (5), 1630–1641, http://dx.doi.org/10.4319/lo.2004.49.5.1630.

Bozec, Y., Thomas, H., Elkalay, K., de Baar, H.J.W., 2005. The continental shelf pump for CO_2 in the North Sea – evidence from summer observation. Mar. Chem. 93 (2–4), 131–147, http://dx.doi.org/10.1016/j.marchem.2004.07.006.

Cai, W.-J., 2011. Estuarine and coastal ocean carbon paradox: CO_2 sinks or sites of terrestrial carbon incineration? Annu. Rev. Mar. Sci. 3, 123–145, http://dx.doi.org/10.1146/annurev-marine-120709-142723.

Donelan, M., Drennan, W., 1995. Direct field measurements of the flux of carbon dioxide. In: Jähne, B., Monahan, E.C. (Eds.), Air-water Gas Transfer. Aeon Ver., Hanau, 677–683.

Doney, S.C., Fabry, V.J., Feely, R.A., Kleypas, J.A., 2009. Ocean acidification: the other CO_2 problem. Annu. Rev. Mar. Sci. 1, 169–192, http://dx.doi.org/10.1146/annurev.marine.010908.163834.

Esters, L., Landwehr, S., Sutherland, G., Bell, T.G., Christensen, K. H., Saltzman, E.S., Miller, S.D., Ward, B., 2017. Parameterizing air-sea gas transfer velocity with dissipation. J. Geophys. Res. 122 (4), 3041–3056, http://dx.doi.org/10.1002/2016JC012088.

Fabry, V.J., Seibel, B.A., Feely, R.A., Orr, J.C., 2008. Impacts of ocean acidification on marine fauna and ecosystem processes. ICES J. Mar. Sci. 65 (3), 414–432, http://dx.doi.org/10.1093/icesjms/fsn048.

Frew, N.M., Nelson, R.K., McGillis, W.R., Edson, J.B., Bock, E.J., Hara, T., 2002. Spatial variations in surface microlayer surfactants and their role in modulating air-sea exchange. In: Gas Transfer at Water Surfaces. American Geophys Union, Washington, DC, 153–159.

Garbe, C.S., Rutgersson, A., Boutin, J., de Leeuw, G., Delille, B., Fairall, C.W., Gruber, N., Hare, J., Ho, D.T., Johnson, M.T., Nightingale, P.D., Pettersson, H., Piskozub, J., Sahlée, E., Tsai, W.-T., Ward, B., Woolf, D.K., Zappa, C.J., 2014. Transfer-across the air-sea interface. In: Liss, P.S., Johnson, M.T. (Eds.), Ocean-Atmosphere Interactions of Gases and Particles. Springer, Heidelberg, 55–112.

Guérin, F., Abril, G., Serça, D., Delon, C., Richard, S., Delmas, R., Tremblay, A., Varfalvy, L., 2007. Gas transfer velocities of CO_2 and CH_4 in a tropical reservoir and its river downstream. J. Mar. Syst. 66 (1–4), 161–172, http://dx.doi.org/10.1016/j.jmarsys.2006.03.019.

Ho, D.T., Law, C.S., Smith, M.J., Schlosser, P., Harvey, M., Hill, P., 2006. Measurements of air-sea gas exchange at high wind speeds in the Southern Ocean: implications for global parameterizations. Geophys. Res. Lett. 33 (16), L16611, http://dx.doi.org/10.1029/2006GL026817.

Ho, D.T., Wanninkhof, R., Schlosser, P., Ullman, D.S., Hebert, D., Sullivan, K.F., 2011. Toward a universal relationship between wind speed and gas exchange: gas transfer velocities measured with $^3He/SF_6$ during the Southern Ocean Gas Exchange Experiment. J. Geophys. Res. 116 (C4), C004F04, http://dx.doi.org/10.1029/2010JC006854.

Hong, H., Shen, R., Zhang, F., Wen, Z., Chang, S., Lin, W., Kranz, S. A., Luo, Y.-W., Kao, S.-J., Morel, F.M., 2017. The complex effects of ocean acidification on the prominent N_2-fixing cyanobacterium *Trichodesmium*. Science 356 (6337), 527–531, http://dx.doi.org/10.1126/science.aal2981.

Jeffery, C.D., Robinson, I.S., Woolf, D.K., 2010. Tuning a physically-based model of the air–sea gas transfer velocity. Ocean Model. 31 (1–2), 28–35, http://dx.doi.org/10.1016/j.ocemod.2009.09.001.

Johnson, M., 2010. A numerical scheme to calculate temperature and salinity dependent air-water transfer velocities for any gas. Ocean Sci. 6 (4), 913–932, http://dx.doi.org/10.5194/os-6-913-2010.

Kilcher, L.F., Thomson, J., Harding, S., Nylund, S., 2017. Turbulence measurements from compliant moorings. Part II: Motion correction. J. Atmos. Ocean Technol. 34, 1249–1266, http://dx.doi.org/10.1175/jtech-d-16-0213.1.

Kilcher, L., Thomson, J., Talbert, J., DeKlerk, A., 2016. Measuring Turbulence from Moored Acoustic Doppler Velocimeters. A Manual to Quantifying Inflow at Tidal Energy Sites. National Renewable Energy Lab., http://dx.doi.org/10.2172/1244672.

Kleemann, M., Meliß, M., 1993. Regenerative Energiequellen: mit 75 Tabellen, 2nd edn. Springer, Berlin.

Kremer, J.N., Nixon, S.W., Buckley, B., Roques, P., 2003. Technical note: Conditions for using the floating chamber method to estimate air-water gas exchange. Estuaries 26, 985–990, http://dx.doi.org/10.1007/BF02803357.

Kroeker, K.J., Kordas, R.L., Crim, R., Hendriks, I.E., Ramajo, L., Singh, G.S., Duarte, C.M., Gattuso, J.P., 2013. Impacts of ocean acidification on marine organisms: quantifying sensitivities and interaction with warming. Glob. Change Biol. 19 (6), 1884–1896, http://dx.doi.org/10.1111/gcb.12179.

Le Quéré, C., Andrew, R.M., Friedlingstein, P., Sitch, S., Hauck, J., Pongratz, J., Pickers, P.A., Korsbakken, J.I., Peters, G.P., Canadell, J.G., Arneth, A., Arora, V.K., Barbero, L., Bastos, A., Bopp, L., Chevallier, F., Chini, L.P., Ciais, P., Doney, S.C., Gkritzalis, T., Goll, D.S., Harris, I., Haverd, V., Hoffman, F.M., Hoppema, M., Houghton, R.A., Hurtt, G., Ilyina, T., Jain, A.K., Johannessen, T., Jones, C.D., Kato, E., Keeling, R.F., Goldewijk, K.K., Landschützer, P., Lefèvre, N., Lienert, S., Liu, Z., Lombardozzi, D., Metzl, N., Munro, D.R., Nabel, J.E.M.S., Nakaoka, S.I., Neill, C., Olsen, A., Ono, T., Patra, P., Peregon, A., Peters, W., Peylin, P., Pfeil, B., Pierrot, D., Poulter, B., Rehder, G., Resplandy, L., Robertson, E., Rocher, M., Rödenbeck, C., Schuster, U., Schwinger, J., Séférian, R., Skjelvan, I., Steinhoff, T., Sutton, A., Tans, P.P., Tian, H., Tilbrook, B., Tubiello, F.N., van der Laan-Luijkx, I.T., van der Werf, G.R., Viovy, N., Walker, A.P., Wiltshire, A.J., Wright, R., Zaehle, S., Zheng, B., 2018. Global Carbon Budget 2018. Earth Syst. Sci. Data 10 (4), 2141–2194, http://dx.doi.org/10.5194/essd-10-2141-2018.

Manzetti, S., Stenersen, J.H.V., 2010. A critical view of the environmental condition of the Sognefjord. Mar. Poll. Bull. 60 (12), 2167–2174, http://dx.doi.org/10.1016/j.marpolbul.2010.09.019.

Mascarenhas, V.J., Voß, D., Wollschlaeger, J., Zielinski, O., 2017. Fjord light regime: bio-optical variability, absorption budget, and hyperspectral light availability in Sognefjord and Trondheimsfjord, Norway. J. Geophys. Res. 122, 3828–3847, http://dx.doi.org/10.1002/2016JC012610.

McGillis, W.R., Edson, J.B., Ware, J.D., Dacey, J.W., Hare, J.E., Fairall, C.W., Wanninkhof, R., 2001. Carbon dioxide flux techniques performed during GasEx-98. Mar. Chem. 75 (4), 267–280, http://dx.doi.org/10.1016/S0304-4203(01)00042-1.

Meire, L., Søgaard, D., Mortensen, J., Meysman, F., Soetaert, K., Arendt, K., Juul-Pedersen, T., Blicher, M., Rysgaard, S., 2015. Glacial meltwater and primary production are drivers of strong CO_2 uptake in fjord and coastal waters adjacent to the Greenland Ice Sheet. Biogeosciences 12 (8), 2347–2363, http://dx.doi.org/10.5194/bg-12-2347-2015.

Mustaffa, N.I.H., Ribas-Ribas, M., Banko-Kubis, H.M., Wurl, O., in preparation. In situ CO_2 transfer velocity reduction by natural surfactants in the sea surface microlayer. Nat. Commun.

Pereira, R., Schneider-Zapp, K., Upstill-Goddard, R.C., 2016. Surfactant control of gas transfer velocity along an offshore coastal transect: results from a laboratory gas exchange tank. Biogeosciences 13 (13), 3981–3989, http://dx.doi.org/10.5194/bg-13-3981-2016.

Pringault, O., Tassas, V., Rochelle-Newall, E., 2007. Consequences of respiration in the light on the determination of production in pelagic systems. Biogeosciences 4 (1), 105–114, http://dx.doi.org/10.5194/bg-4-105-2007.

Quinn, G.P., Keough, M.J., 2009. Experimental Design and Data Analysis for Biologists. Cambridge Univ. Press, New York, 537 pp.

R Core Team, 2017. R: A Language and Environment for Statistical Computing. R Foundation for Statistical Computing, Vienna, Austria.

Raymond, P.A., Cole, J.J., 2001. Gas exchange in rivers and estuaries: choosing a gas transfer velocity. Estuaries 24 (2), 312–317, http://dx.doi.org/10.2307/1352954.

Ribas-Ribas, M., Helleis, F., Rahlff, J., Wurl, O., 2018a. Air-sea CO_2-exchange in a large annular wind-wave tank and the effects of surfactants. Front. Mar. Sci. 5, 457, http://dx.doi.org/10.3389/fmars.2018.00457.

Ribas-Ribas, M., Kilcher, L., Wurl, O., 2018b. Sniffle: A step forward to measure in situ CO_2 fluxes with the floating chamber tech-

nique. Elementa 6 (1), 14, http://dx.doi.org/10.1525/elementa.275.

Ribas-Ribas, M., Mustaffa, N.I.H., Rahlff, J., Stolle, C., Wurl, O., 2017. Sea Surface Scanner (S3): A catamaran for high-resolution measurements of biogeochemical properties of the sea surface microlayer. J. Atmos. Oceanic Technol. 34 (7), 1433—1448, http://dx.doi.org/10.1175/jtech-d-17-0017.1.

Romano, J.-C., 1996. Sea-surface slick occurrence in the open sea (Mediterranean, Red Sea, Indian Ocean) in relation to wind speed. Deep-Sea Res. Pt. I 43 (4), 411—423, http://dx.doi.org/10.1016/0967-0637(96)00024-6.

Rutgersson, A., Smedman, A., 2010. Enhanced air—sea CO_2 transfer due to water-side convection. J. Mar. Syst. 80 (1—2), 125—134, http://dx.doi.org/10.1016/j.jmarsys.2009.11.004.

Sætre, R., Aure, J., Danielssen, D., 2003. Long-term hydrographic variability patterns off the Norwegian coast and in the Skagerrak. ICES Marine Sci. Sym. 150—159.

Schlitzer, R., 2017. Ocean Data View. Ver 5.0.0., https://odv.awi.de/.

Skagseth, Ø., Drinkwater, K.F., Terrile, E., 2011. Wind- and buoyancy-induced transport of the Norwegian Coastal Current in the Barents Sea. J. Geophys. Res.-Oceans 116 (C8), C08007, http://dx.doi.org/10.1029/2011JC006996.

Smith, R.W., Bianchi, T.S., Allison, M., Savage, C., Galy, V., 2015. High rates of organic carbon burial in fjord sediments globally. Nat. Geosci. 8, 450—453, http://dx.doi.org/10.1038/NGEO2421.

Spiess, A.-N., Neumeyer, N., 2010. An evaluation of R^2 as an inadequate measure for nonlinear models in pharmacological and biochemical research: a Monte Carlo approach. BMC Pharmacology 10 (1), 6, http://dx.doi.org/10.1186/1471-2210-10-6.

Stigebrandt, A., 2012. Hydrodynamics and circulation of fjords. I. In: Bengtsson, L., Herschy, R.W., Fairbridge, R.W. (Eds.), Encyclopedia of Lakes and Reservoirs. Springer Netherlands, Dordrecht, 327—344.

Syvitski, J.P.M., Burrell, D.C., Skei, J.M., 1987. Fjords. Processes and Products. Springer, New York, 215 pp.

Takahashi, T., Sutherland, S.C., Wanninkhof, R., Sweeney, C., Feely, R.A., Chipman, D.W., Hales, B., Friederich, G., Chavez, F., Sabine, C., 2009. Climatological mean and decadal change in surface ocean pCO_2, and net sea—air CO_2 flux over the global oceans. Deep-Sea Res. Pt. II 56 (8—10), 554—577, http://dx.doi.org/10.1016/j.dsr2.2008.12.009.

Tokoro, T., Watanabe, A., Kayanne, H., Nadaoka, K., Tamura, H., Nozaki, K., Kato, K., Negishi, A., 2007. Measurement of air—water CO_2 transfer at four coastal sites using a chamber method. J. Mar. Syst. 66 (1—4), 140—149, http://dx.doi.org/10.1016/j.jmarsys.2006.04.010.

Torres, R., Pantoja, S., Harada, N., González, H.E., Daneri, G., Frangopulos, M., Rutllant, J.A., Duarte, C.M., Rúiz-Halpern, S., Mayol, E., Fukasawa, M., 2011. Air-sea CO_2 fluxes along the coast of Chile: from CO_2 outgassing in central northern upwelling waters to CO_2 uptake in southern Patagonian fjords. J. Geophys. Res.-Oceans 116 (C9), C09006, http://dx.doi.org/10.1029/2010JC006344.

Vachon, D., Prairie, Y.T., Cole, J.J., 2010. The relationship between near-surface turbulence and gas transfer velocity in freshwater systems and its implications for floating chamber measurements of gas exchange. Limnol. Oceanogr. 55 (4), 1723—1732, http://dx.doi.org/10.4319/lo.2010.55.4.1723.

Wanninkhof, R., 1992. Relationship between wind speed and gas exchange over the ocean. J. Geophys. Res. 97, 7373—7382.

Wanninkhof, R., 2014. Relationship between wind speed and gas exchange over the ocean revisited. Limnol. Oceanogr 12 (6), 351—362, http://dx.doi.org/10.4319/lom.2014.12.351.

Wanninkhof, R., Asher, W.E., Ho, D.T., Sweeney, C., McGillis, W.R., 2009. Advances in quantifying air-sea gas exchange and environmental forcing. Annu. Rev. Mar. Sci. 1, 213—244, http://dx.doi.org/10.1146/annurev.marine.010908.163742.

Weiss, R.F., 1974. Carbon dioxide in water and seawater: the solubility of a non-ideal gas. Mar. Chem. 2 (3), 203—215, http://dx.doi.org/10.1016/0304-4203(74)90015-2.

Wurl, O., Wurl, E., Miller, L., Johnson, K., Vagle, S., 2011. Formation and global distribution of sea-surface microlayers. Biogeosciences 8 (1), 121—135, http://dx.doi.org/10.5194/bg-8-121-2011.

Zappa, C.J., McGillis, W.R., Raymond, P.A., Edson, J.B., Hintsa, E.J., Zemmelink, H.J., Dacey, J.W.H., Ho, D.T., 2007. Environmental turbulent mixing controls on air-water gas exchange in marine and aquatic systems. Geophys. Res. Lett. 34 (10), L01601, http://dx.doi.org/10.1029/2006GL028790.

Zappa, C.J., Raymond, P.A., Terray, E.A., McGillis, W.R., 2003. Variation in surface turbulence and the gas transfer velocity over a tidal cycle in a macro-tidal estuary. Estuaries 26 (6), 1401-1415, http://dx.doi.org/10.1007/BF02803649.

Zhang, X., Cai, W.-J., 2007. On some biases of estimating the global distribution of air-sea CO_2 flux by bulk parameterizations. Geophys. Res. Lett. 34 (1), L01608, http://dx.doi.org/10.1029/2006GL027337.